Article

Cell atlas of trabecular meshwork in glaucomatous non-human primates and DEGs related to tissue contract based on single-cell transcriptomics

Xu Jia, Jian Wu, Xiaohong Chen, ..., Caibin Deng, Wenru Su, Yehong Zhuo

suwr3@mail.sysu.edu.cn (W.S.)
zhuoyh@mail.sysu.edu.cn (Y.Z.)

Highlights

Establish a cell atlas for trabecular meshwork (TM) of glaucoma and healthy macaques

Showed the detailed features of microstructural alterations in TM of POAG macaques

Explore the differentially expressed genes and pathways with the dysfunction of TM

Illustrate that systolic dysfunction may play an essential role in developing POAG

Article

Cell atlas of trabecular meshwork in glaucomatous non-human primates and DEGs related to tissue contract based on single-cell transcriptomics

Xu Jia,[1,2,5] Jian Wu,[3,4,5] Xiaohong Chen,[1,5] Simeng Hou,[3,4] Yangyang Li,[1] Ling Zhao,[1] Yingting Zhu,[1] Zhidong Li,[1] Caibin Deng,[1] Wenru Su,[1,*] and Yehong Zhuo[1,6,*]

SUMMARY

As the major channel of aqueous humor outflow, dysfunction of trabecular meshwork (TM) can lead to intraocular pressure elevating, which can trigger primary open-angle glaucoma (POAG). In this study, we use single-cell RNA sequencing (scRNA-seq) technique to build an atlas and further explore the spontaneous POAG and healthy macaques cellular heterogeneity associated with the dysfunction of TM contraction. We built the TM atlas, which identified 14 different cell types. In Beam A, Beam B, Beam C, and smooth muscle cell (SMC) cell types, we first found multiple genes associated with TM contraction (e.g., TPM1, ACTC1, TNNT1), determining their differential expression in the POAG and healthy groups. In addition, the microstructural alterations in TM of POAG non-human primates were observed, which was compact and collapsed. Thus, our study indicated that TPM1 may be a key target for regulating TM structure, contraction function, and resistance of aqueous humor outflow.

INTRODUCTION

Elevated intraocular pressure (IOP) is the leading cause of optic nerve injury in glaucoma,[1,2] and effective reduction of IOP is currently recognized as the only effective method to alleviate the progression of glaucoma.[3] As an essential tissue to maintain IOP, the aqueous outflow channel's trabecular meshwork (TM) is critical in regulating aqueous outflow resistance.[4,5] IOP elevation induced by compromised TM outflow is the major cause of primary open-angle glaucoma (POAG) and progressive glaucomatous optic nerve injury.[6,7] However, the mechanism of TM related to elevated IOP is not well understood, leaving limited therapeutic approaches and effective results in controlling IOP. As the main pathway for aqueous outflow, the sieve-like structure of TM regulates aqueous outflow resistance. Clinically, using cholinergic drugs for POAG can indirectly expand the TM sieve-like structure by contracting the ciliary muscle, increasing aqueous humor outflow, and lowering the IOP.[8] However, this theory failed to explain the many occasions that traction of ciliary muscles cannot control IOP. The sieve-like structure of TM has been reported to have relaxation and contraction characteristics after mechanical stress, as well as an actin cytoskeleton structure.[9] These characteristics facilitate the regulation of the aqueous humor outflow through the sieve pore, thus maintaining the stability of IOP. Though dysfunction of the sieve-like structure leads to the increased outflow resistance of the aqueous humor, little is understood about related cell types and pathogenesis in this region. The TM tissue has been proven to have smooth muscle and fibroblast cells, which have an elastic feature. Thus, we postulate that the TM tissue may have contractile properties itself in addition to ciliary muscle affection.

Single-cell RNA sequencing (scRNA-seq) is a novel technology for analyzing the behavior mechanism of single cells and their relationship with the body. It can reveal the gene structure and gene expression level of a single cell, reflecting the heterogeneity between cells and analyzing the contribution of a single cell to the entire organ.[10,11] To explore the cell types and related genes and pathways involved in the relaxation and contraction of the sieve pore of TM in POAG, we screened spontaneous POAG monkey models. We analyzed the scRNA-seq results and the healthy controls in our study. Having carefully compared the two groups in cell types, cell proportion, and differentially expressed genes (DEGs), we unveiled the principal pathways regulating the aqueous outflow in the TM tissue. Moreover, we have also studied these genes through histology and molecular biology to understand their expressions and functions in TM tissue. Our results may provide the necessary theoretical basis for POAG precision treatment and novel drug development.

[1]State Key Laboratory of Ophthalmology, Zhongshan Ophthalmic Center, Sun Yat-sen University, Guangdong Provincial Key Laboratory of Ophthalmology Visual Science, Guangzhou, Guangdong, China
[2]The Affiliated Hospital of Guizhou Medical University, Guiyang, Guizhou, China
[3]Beijing Tongren Eye Center, Beijing Tongren Hospital, Capital Medical University, Beijing, China
[4]Beijing Ophthalmology & Visual Sciences Key Laboratory, Beijing, China
[5]These authors contributed equally
[6]Lead contact
*Correspondence: suwr3@mail.sysu.edu.cn (W.S.), zhuoyh@mail.sysu.edu.cn (Y.Z.)
https://doi.org/10.1016/j.isci.2023.108024

Table 1. Basic information of animal models in the study

No.	Age (y)	Sex	Mean IOP (mm/Hg, Tono-vet)		Diagnosis
			OD	OS	
1	18	Female	27 ± 3.72	28 ± 1.78	POAG
2	17	Female	30 ± 2.13	29 ± 2.35	POAG
3	16	Female	29 ± 2.88	31 ± 2.75	POAG
4	16	Female	16 ± 1.56	15 ± 1.05	Healthy
5	17	Female	15 ± 0.93	18 ± 0.61	Healthy
6	16	Female	18 ± 0.75	16 ± 0.82	Healthy

RESULTS

Screening of spontaneous POAG monkeys

To screen for the spontaneous monkeys with POAG characteristics, we examined more than 600 cynomolgus macaque monkeys with Tono-Vet to measure IOP, slit-lamp, gonioscopy, fundus photos, and optical coherence tomography (OCT). Finally, we identified 3 monkeys as spontaneous POAG models, as well as 3 healthy monkeys with similar demographic characteristics that were used as controls (Table 1). Subsequently, we figured out significant similarities in POAG characteristics between monkeys and humans in abnormally elevated IOP, deep anterior chamber, wide atrial angle, sizable cup-to-disc ratio, concave lamina cribrosa, and retinal nerve fiber layer (RNFL) thinning (Figure 1, Step 2). Among these characters, the IOP, cup/disk (C/D) ratio, and RNFL thickness were all statistically different between the POAG monkeys and their healthy controls (Table 2).

Single-cell transcriptome map of TM between glaucoma and healthy monkeys

In the POAG group, the median unique molecular identifier (UMI) count per cell was 2,746, the estimated number of cells was 10,624, and the total number of genes detected was 17,374. In the control group, the median UMI count per cell was 2,317, the estimated number of cells was 13,785, and the total number of genes detected was 17,682. After applying the quality control indicators, we obtained 8,759 cells (14,368 genes) in the POAG group and 9,023 cells (16,763 genes) in the control group. Then, we identified 14 clusters by applying Seurat software for clustering analysis, and cell homology was found using cluster-specific genes and typical cell type markers (Figures 2A, B, and 2C). The cell types include Beam A cell, Beam B cell, Beam C cell, smooth muscle cell (SMC), myelinating Schwann (Schmy) cell, nonmyelinating Schwann (SchNmy) cell, vascular endothelium (Vendo), macrophages, Schlemm's canal (SC) cell, pericytes cell, T/NK cell, juxtacanalicular tissue (JCT) cell, and melanocyte. The control group consisted of the same cell types as the POAG group. Beam cell clusters predominantly express fibroblast-related genes. According to their specific expressed genes including fibroblast characteristics, we divided beam cells into Beam A, Beam B, and Beam C. By analysis of the proportion of each cell cluster, Beam cells account for the most significant proportion in TM. The proportion of Beam A was lower in the POAG group than that in the control group, while the proportion of Beam C was higher in the POAG group than that in the control group. SMC was also an essential part of the tissue, and the proportion in the POAG group was lower than that in the control group (Figure 2D). The proportion of JCT was lower in the POAG group than that in the control group. The proportion of SC was significantly higher in the POAG group than that in the control group, and the proportion of epithelium was significantly lower in the POAG group than that in the control group.

To further investigate how genes contribute to the pathogenesis of POAG, we mapped the expression of POAG-associated disease genes in the spontaneous glaucoma monkey and control groups (Figure 2E). For this analysis, we deliberately selected specific genes that have been previously reported in the literature as having a robust association with POAG.[12–14] In particular, our observations revealed that genes associated with open-angle glaucoma (e.g., MYOC, OPTN) are relatively more highly expressed in the glaucoma group. Those genes associated with IOP (e.g., CAV1/CAV2, TMCO1) also demonstrated the same expression increase in the glaucoma group.

Functional enrichment analysis of DEGs in each cell cluster

We have done functional enrichment analysis using the methods of Gene Ontology (GO) biological processes, Kyoto Encyclopedia of Genes and Genomes (KEGG) pathway, Reactome gene sets, Wiki pathways, etc., to detect the genes or pathways associated with abnormal TM function in each cluster. Cell clusters of Beams had fibroblast characteristics, and the Beams cell and SMC with contractile features became the focus of our enrichment analysis. In the results, we saw a fascinating phenomenon. In Beam A, Beam B, Beam C, and SMC clusters, DEGs were enriched in genes and pathways associated with tissue contraction multiple times, including "Smooth Muscle Contraction" (R-HSA-445355), "Molecules associated with elastic fibers" (R-HSA-2129379), "Myometrial relaxation and contraction pathways" (WP289), "Striated muscle contraction pathway" (WP383), "actin cytoskeleton organization" (GO:0030036), and "muscle structure development" (GO:0061061) (Figure 3). Among these pathways, the TPM gene attracted our attention. Utilizing KEGG pathway analysis (David's website), we discovered that the TPM gene is present in a pathway associated with tissue contraction, including TPM, ACTC, TNNT, etc. (Figure 4A). Having re-analyzed TM clusters, we discovered that TPM, ACTC1, and TNNT1 were mainly located in Beams
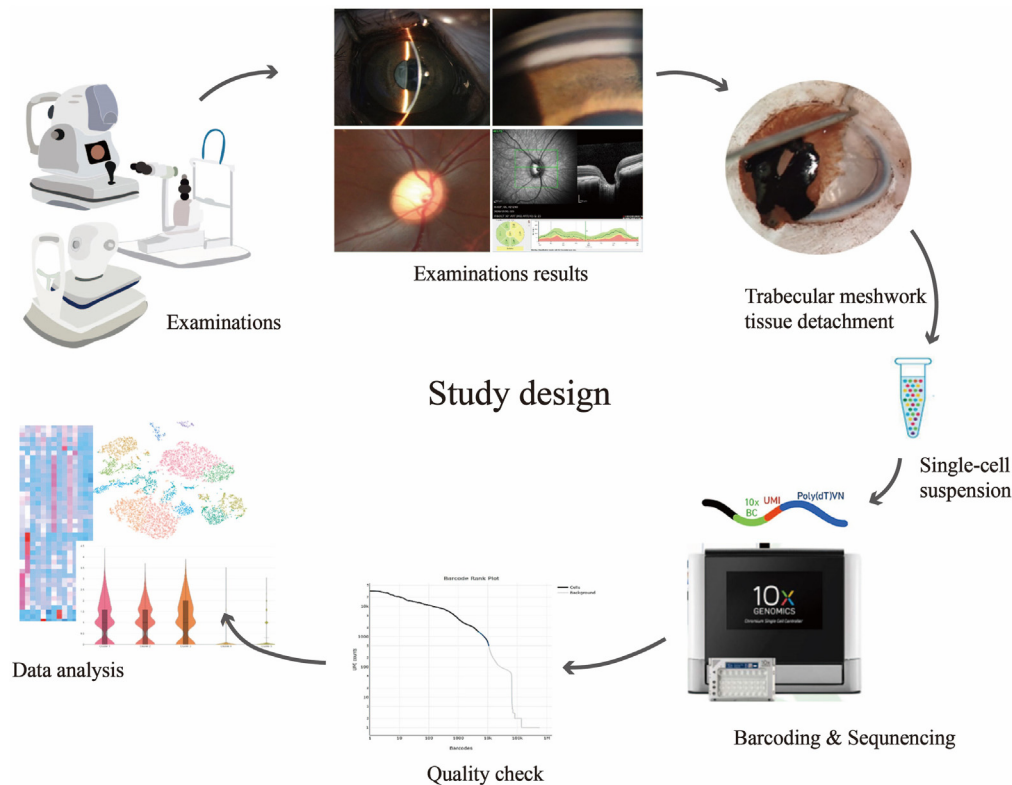
Figure 1. Workflow in constructing trabecular meshwork cell atlas for non-human primates with POAG
Step 1–2: Slit-lamp exam, gonioscope exam, fundus imaging as well as OCT were utilized to screen for spontaneous POAG models, which according with diagnostic criteria of POAG in humans. Step 3: TM tissues were detached integrally from inner surface of eyeball. Step 4: These figures illustrates the general process of single-cell sequencing and analysis.

and SMC clusters (Figures 4B–4E). TPM encodes a widely distributed tropomyosin that regulates various types of muscle relaxation and contraction functions in conjunction with TNNT/ACTC.[15] In cardiovascular disease research, it has been revealed that increasing TPM expression levels is accompanied by increased expression levels of TNNT1 and ACTC1, inducing cardiomyocyte contractile dysfunction as well as diminished vessel dilation.[16,17] Based on these reports, we preliminarily explored the expression localization and correlation relationship of these three genes in this study.

Immunohistochemical localization of TPM, TNNT1, and ACTC1 in TM tissues of monkeys

We have performed immunohistology of TPM1 in the left eyes of POAG monkeys and the healthy controls. The results showed that TPM1 was expressed in the sieve-like region of the TM tissue. The AOD value was obtained by ImageJ software, showing a lower expression level in the glaucoma group than in the healthy group ($p < 0.05$). ACTC1 and TNNT1 expressions were detected by immunofluorescence in the left eyes of POAG monkeys and healthy controls. ACTC1 and TNNT1 were also expressed in the sieve-like region of the TM tissue. The AOD values of ACTC1 and TNNT1 were lower in the glaucoma group than in the healthy group ($p < 0.05$) (Figure 5).

In the observation of histological sections, we additionally found that there were significant alterations in the tissue structure of the TM region in the disease group (Figure 6A). The sieve-like region of TM was compact and collapsed in the POAG models not just thin, especially in the anterior section. Due to the sample limitations in previous histological studies, this result was a novel finding for structural changes in the TM closest to human glaucoma.

qPCR verification about TPM1, ACTC1, and TNNT1 from human TM cells

By transfecting normal human TM cells with TPM1 overexpression gene, the expression level of TPM1 in TM cells increased ($p < 0.05$). Transfecting normal human TM cells with TPM1 suppressor expression gene, the expression level of TPM1 in TM cells was decreased ($p < 0.05$). In the elevated TPM1 expression group, the expression level of ACTC1 was significantly increased ($p < 0.05$). Similarly, the expression level of TNNT1 also demonstrated an increase. In the group with decreased TPM1 expression, the expression level of ACTC1 was decreased compared to the normal group ($p < 0.05$), and the expression level of TNNT1 was significantly decreased ($p < 0.05$) (Figures 6B–6D).

Table 2. Demographic data and ocular parameters of glaucoma and control group

Variables	Glaucoma (N = 3)	Control (N = 3)	p value
Sex (%)			
Male	0	0	
Female	100	100	
Age (yrs)	17.00 ± 0.82	16.33 ± 0.47	0.070
IOP (mmHg)			
OD	28.67 ± 2.65	17.02 ± 1.15	**<0.001**
OS	29.33 ± 2.37	16.33 ± 0.78	**<0.001**
Average RNFL thickness (μm)	86.21 ± 4.31	96.56 ± 5.27	**0.035**
Lamina cribrosa thickness (μm)	326.36 ± 27.02	241.28 ± 45.33	**0.003**
Anterior laminar insertion depth (μm)	296.13 ± 22.75	222.86 ± 53.69	**0.029**
C/D ratio	0.76 ± 0.12	0.35 ± 0.08	**0.001**

All data were shown as M± SD or n (%). IOP, intraocular pressure; RNFL, retinal nerve fiber layer. All p values less than 0.05 are bolded.

Western blot verification about TPM1, ACTC1, and TNNT1 from human TM cells

By transfecting normal human TM cells with TPM1 overexpression gene, the expression level of TPM1 protein in TM cells was increased. Transfecting normal human TM cells with TPM1 suppressor expression gene, the expression level of TPM1 protein in TM cells decreased. In the elevated TPM1 expression group, the expression level of ACTC1 protein was considerably increased, and the expression level of TNNT1 protein was also increased. In the group with reduced TPM1 expression, the expression level of ACTC1 protein decreased compared to the normal group, and the expression level of TNNT1 protein was significantly decreased (Figures 6E and 6F).

DISCUSSION

In order to figure out the pathogenesis of POAG, previous research has established animal models of POAG with ocular hypertension by TM laser or drug injection in the anterior chamber.[18,19] However, animal models with these methods cannot simulate the actual situation of naturally occurring POAG in humans, making the representativeness of the results questionable. In this study, three spontaneous POAG monkeys and the healthy controls were carefully examined by slit-lamp microscope, gonioscopy, fundus photography, and OCT. Through the examination, we found significant similarities between monkeys and human beings in POAG characteristics. For example, both have a wide atrial angle and the anterior chamber, increased cup-to-disc ratio, concave sieve plate, and RNFL thinning. Therefore, single-cell sequencing in spontaneous POAG monkeys could provide valuable information for the pathogenesis of POAG in human beings. scRNA-seq research of normal human TM cells has previously been performed. However, in this study, we performed the scRNA-seq research in non-human primate POAG model and compared the results with normal animals for the first time. By performing scRNA-seq on the TM cells of monkeys, the cell maps of POAG and healthy monkeys were generated. By querying the gene markers from the literature and the website (PanglaoDB, GeneCard), we identified 14 cell types in the TM tissue, which are consistent with previous studies.[20,21] The cell types in POAG TM coincide with normal models, while the proportion of each cell cluster was different between the two groups. The proportions of Beam A and Beam C were markedly different. The proportion of Beam A was lower in the POAG group than in the control group. In comparison, the proportion of Beam C was higher in the POAG group than in the control group. Beam clusters represented the cytoskeletal component of TM. They were the most abundant in TM, and alterations in the proportion of these two cell clusters may have an important impact on TM tissue function abnormalities, which requires further exploration in future research. The proportion of SC was significantly increased in the POAG group. Since SC is an essential channel of aqueous humor outflow, whether the increased cell number is associated with increased outflow resistance deserves further exploration in future research. Previous studies have suggested that extracellular matrix reorganization and TM fibrosis were the leading causes of increased resistance to aqueous humor outflow.[22,23] However, evidence suggested that TM itself had contractile characteristics and that aqueous drainage was the result of active contraction of the TM.[24,25] TM's abnormal relaxation and contraction function may be another important factor leading to aqueous humor drainage disorders. SMC is a vital part of the TM, which is closely related to the contractile function of TM. The proportion of SMC is decreased in the POAG TM, which may be one of the decisive factors for the contractile dysfunction of TM tissue. Indeed, beam cells with fibroblastic features also have elastic contractile functions.[26,27] Therefore, detailed studies on these several cell types can serve to explore the mechanisms responsible for contractile dysfunction of TM.

    In the results of DEGs enrichment analysis, we discovered that DEGs in clusters of Beams and SMC were enriched in some genes and pathways associated with some tissue contraction functions (details in result part). Among these pathways, the TPM1 gene attracted our attention. TPM1, a member of the tropomyosin family of highly conserved, is widely distributed actin-binding proteins involved in the contractile system of striated and smooth muscles and the cytoskeleton of non-muscle cells. It is composed of two alpha-helical chains arranged as a coiled coil. It is polymerized end to end along the two grooves of actin filaments; TPM1 provides stability to the filaments. The encoded protein is one type of alpha-helical chain that forms the predominant tropomyosin of striated muscle. It also functions with the troponin complex to regulate
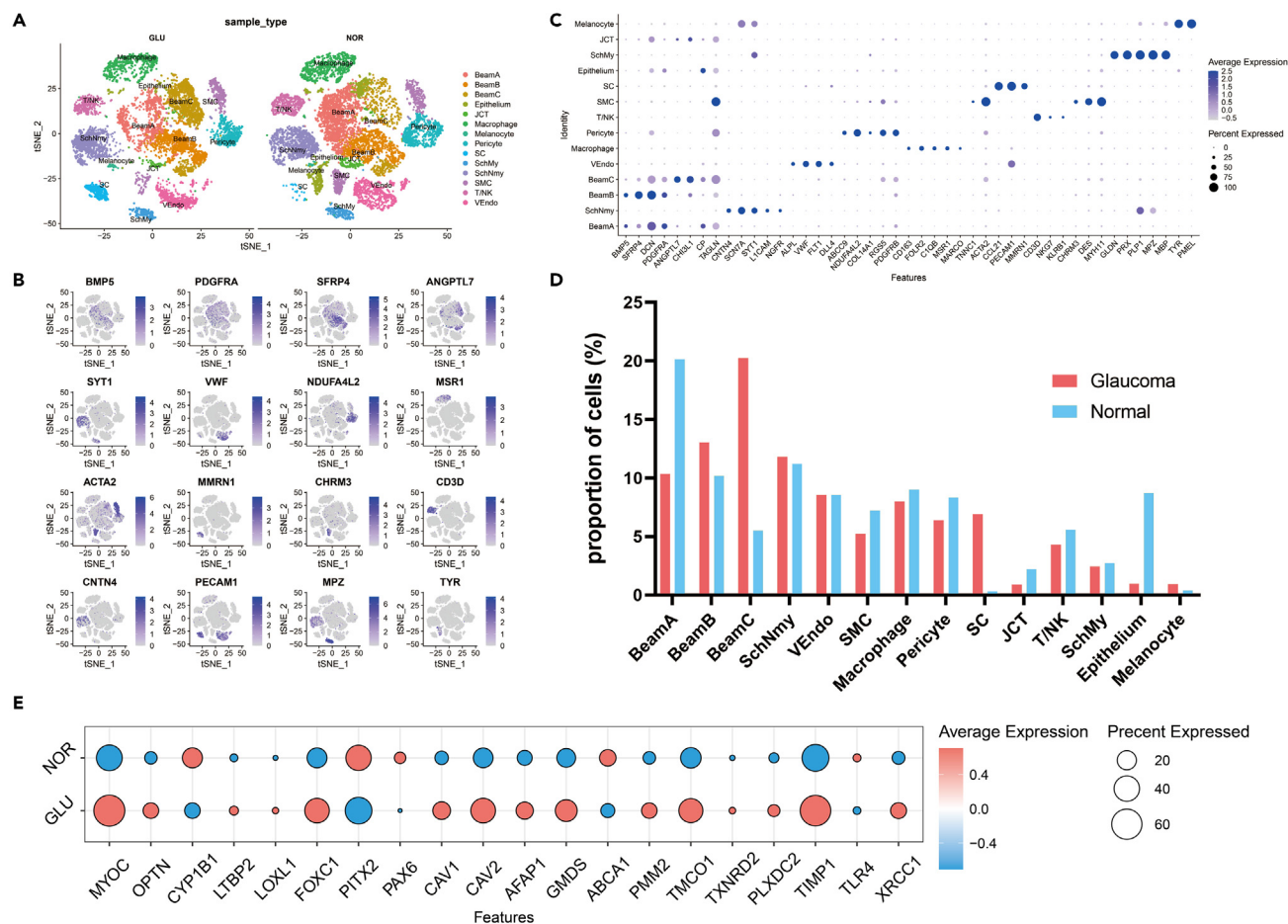
Figure 2. Cell types and gene expression in the macaques trabecular meshwork cells

(A) Cell atlas in TM between spontaneous POAG and healthy macaques.

(B) Feature-plot of marker gene expression that showed the distribution of each cell cluster in the cell atlas.

(C) Dot-plot of marker gene expression combinations that identified type of each cell cluster.

(D) Difference of cells' proportions in each cell cluster between POAG and healthy macaques.

(E) Dot-plot of the POAG-associated disease genes' expression level between POAG and healthy macaques.

the calcium-dependent interaction of actin and myosin during muscle contraction. In smooth muscle and non-muscle cells, alternatively spliced transcript variants encoding a range of isoforms have been described.[28,29]

The current study confirmed that ACTC1 and TNNT1 have a positive regulatory effect on the contractile function of various muscle tissues and fibrous tissues.[30–32] In the study of various cardiovascular diseases, it was revealed that there was a close linkage between TPM1, ACTC1, and TNNT1, which could regulate the contractile function of numerous muscle tissues.[33] However, different research results on the altered expression levels of TPM1 were inconsistent. Some studies suggest that increased TPM1 leads to decreased expression levels of ACTC1 as well as TNNT1,[16] and other studies have suggested that inhibition of TPM expression level could cause abnormal tissue contractile function.[34] It is believed that TPM is expected to be a key target for the treatment of various muscle contraction-related diseases.[17] Therefore, more experiments are required to verify the effect of altered TPM1 expression on tissue contractile function.

The effects of TPM on ocular tissues have rarely been studied. Only studies on the lens found that TPM played a crucial role in maintaining lens physiology and morphology.[35] In this study, we localized TPM1 by immunohistochemistry and found that it was mainly expressed in the cribriform structure of TM. Likewise, ACTC1 and TNNT1 were also mainly expressed in the cribriform structure of TM. The expression level of these three genes in the disease group was lower than that in the normal group. To preliminarily explore the effect of altered expression of TPM1 on ACTC1 and TNNT1 expression in human TM cells, we used qPCR experiments to identify that ACTC1 and TNNT1 expression levels increased accompanied by up expression of TPM1. Similarly, expression levels of ACTC1 and TNNT1 decreased, accompanied by a down expression of TPM1. Combined with tissues derived from spontaneous POAG monkeys, we concluded that this histological difference in expression was consistent with previous studies.
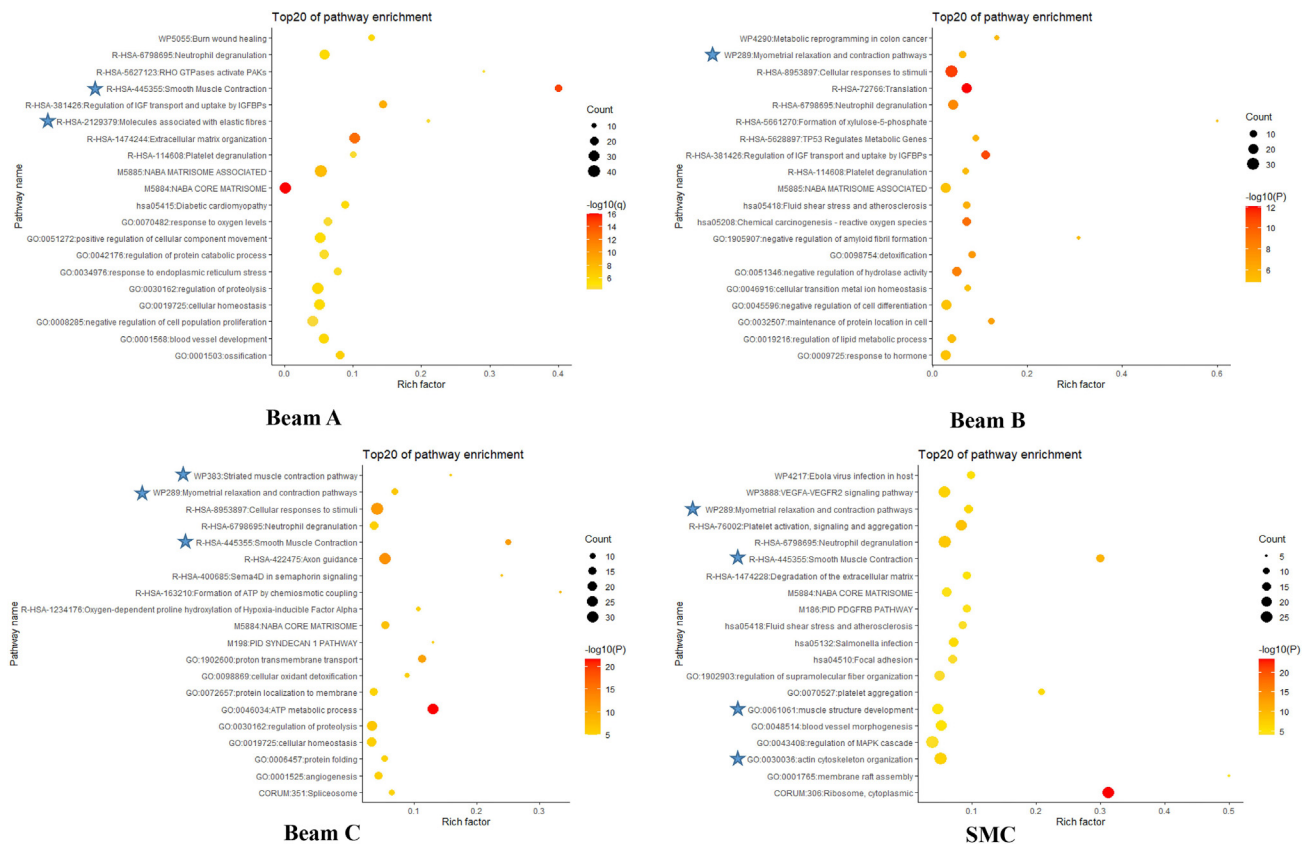
Figure 3. Functional enrichment analysis of DEGs in Beam A, Beam B, Beam C, and SMC clusters
Multiple genes and pathways associated with tissue contraction function were identified in these four cell clusters (annotation with pentagram).

In this study, we found significant differences in the sieve-like region of TM between POAG and normal animals by histological sectioning. The TM not only became thinner, but the structure became compact due to collapse. There have been many previous studies on the structure of TM in POAG, but most of the studies have been based on glucocorticoids, transforming growth factor (TGF)-β2, lasers, and other methods to model rodents,[36–38] and their consistency with spontaneous POAG is difficult to verify. Previous studies have suggested that TM tissue becomes thinner when POAG occurs; however our study found that thinning of the TM does not simply reduce the tissue component but becomes compact caused by collapsed tissue structure. It is difficult to obtain tissue sheet sections from intact eyeballs in human disease samples for organization study and difficult to truly understand the exact trend of TM structure changes in POAG patients. Combined with the abnormal genes related to relaxation and contraction function in various cell types in TM with POAG macaque found in this study, which pathologic features are highly consistent with human beings, we believed that the cause of TM structural changes is not only tissue proliferation, fibrosis, and other factors considered previously but also TM relaxation and contraction dysfunction, which may be the main reason for TM structural changes and increased resistance to aqueous humor outflow. This finding also suggests that in establishing the animal model of POAG, induced ocular hypertension does not well represent the pathomechanisms of POAG. Instead, more attention should be paid to the leading cause of TM structure collapse.

There were two previous studies which demonstrated the preliminary explorations of single-cell sequencing studies based on normal human or animal eye trabecular reticulum tissue. With clustered cells and identified markers for various types of cells, various types of cells were also localized through histological experiments. However, our study differs from these two studies in many ways. In our study, non-human primates of spontaneous POAG in nature detected by screening were used as the study object. These animals' clinical manifestations and pathological features are highly consistent with human POAG. In previous studies, POAG human eye clinical tissue samples were difficult to obtain for basic research. Moreover, rodents have a markedly different trabecular mesh structure from humans. At the same time, many glaucoma models were obtained by blocking the trabecular mesh with drugs, lasers, etc., which are not POAGs, but secondary glaucoma models. Therefore, cynomolgus monkeys with high homology to human genes were used as the research object to perform single-cell sequencing of their trabecular mesh. The single-cell transcriptome data obtained are invaluable. We further compared the differences in cellular heterogeneity between naturally occurring POAG and normal cynomolgus monkeys. Moreover, through enrichment analysis, it was found that multiple cell types were involved in regulating tissue contraction function (Previous studies have suggested that the disorder of drainage of aqueous humor in patients with POAG is mainly due to obstruction of channels. However, some studies believe that the
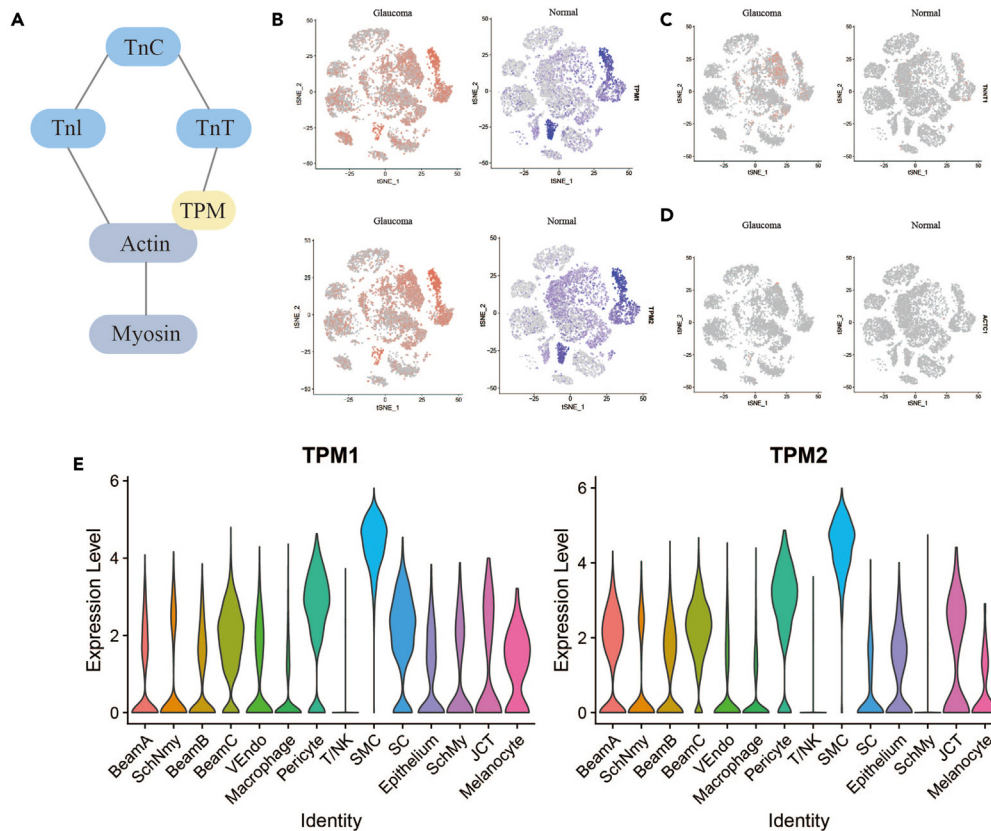
Figure 4. Exploring the pathway associated with tissue contraction
(A) The diagram of smooth muscle contract pathway, in which the relationship between TPM, ACTC, and TNNT1 was shown.
(B–E) Feature-plot and violin-plot of genes that showed TPM1, ACTC1, and TNNT1 mainly located in the Beams and SMC clusters.

abnormal function of the trabecular mesh is not just a blockage of the aqueous humor outflow channel. Instead, it is also related to abnormal auto contraction. However, due to the limitations of the research samples, the exploration of relevant genes and pathways has not been very smooth). After further exploration, it was found that this phenomenon may be related to the abnormal contractile function of trabecular mesh, TPM1 gene, and related pathways. Considering the species diversity, we identified the TPM1 expression in human aqueous humor outflow pathways. The results are better representative of the mechanisms of human disease. The POAG single-cell transcriptome data of this study are precious and can be further explored by the majority of researchers to discover more meaningful pathogenic genes and pathways. The results suggest that systolic dysfunction may play an essential role in developing POAG.

TM is an essential channel of aqueous humor drainage, while abnormal structure and function of TM are important causes of elevated IOP and POAG. For cell types of TM that are diverse and structurally delicate, single-cell sequencing methods can better identify cell types and explore disease-related genes and pathways in diverse cell clusters. We believe that the clinical features and cell types of TM in spontaneous POAG monkeys were highly consistent with those in humans, which could well represent the study of POAG pathogenesis in humans. The proportion of some cell clusters and the structure of TM tissues were significantly different between POAG and normal models, suggesting that there may be a close relationship between the change in cell proportion and the abnormality of tissue structure. Some genes and pathways related to tissue contraction were detected in DEGs enrichment analysis of Beams and SMC, of which TPM1 was focused on because of its important roles in tissue relaxation and contraction function. It was first found that TPM1 was mainly localized to the sieve structure of TM. Moreover, there were differences in expression between the disease and regular models. By regulating the expression of TPM1, the expression levels of ACTC1 and TNNT1, which regulate tissue contraction, were significantly changed, suggesting that TPM1 may be a therapeutic target for regulating the contractile function of TM. Further research will validate its effects in POAG animal models and explore new treatment approaches.

Limitations of the study

There are also some limitations in this study. Firstly, since the spontaneous POAG model in non-human primate cynomolgus was limited, the amount of the sample may not be enough. Meanwhile, as the artificial animal model of glaucoma used has the same pathogenesis as
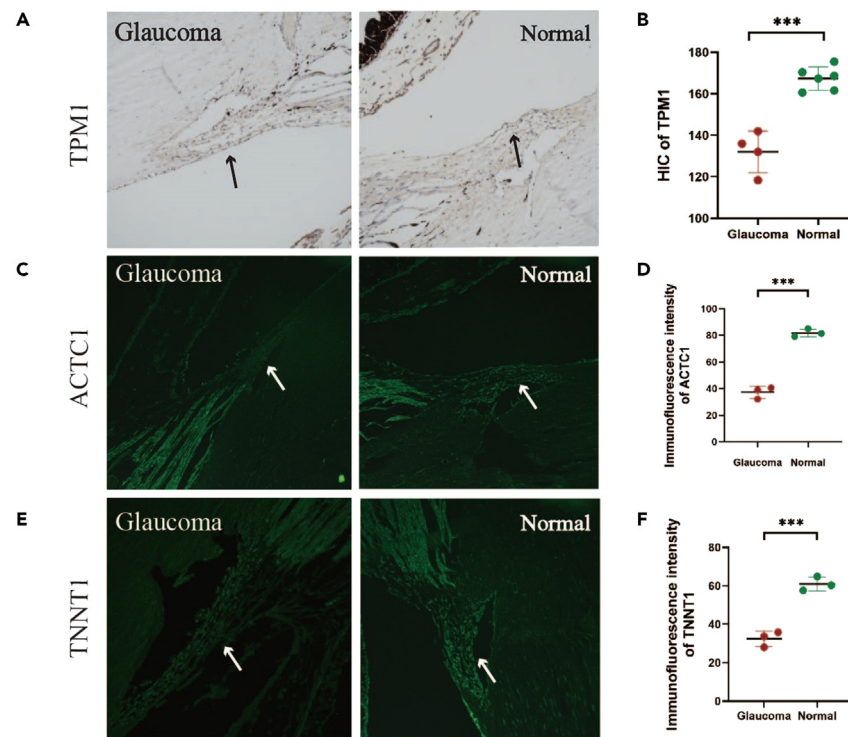
Figure 5. Immunohistochemical localization of TPM, TNNT1, and ACTC1 in the macaques' TM tissues

(A and B) Results of immunohistochemistry. The TPM1 was expressed in the sieve-like structure of TM, and the expression level was lower in POAG tissues than that in normal tissues (p < 0.01).

(C and D) Results of immunofluorescence. The ACTC1 was expressed in the sieve-like structure of TM, and the expression level was lower in POAG tissues than in normal tissues (p < 0.01).

(E and F) Results of immunofluorescence. The TNNT1 was expressed in the sieve-like structure of TM, and the expression level was lower in POAG tissues than in normal tissues (p < 0.01). White arrows point to the sieve-like structure of TM.

secondary glaucoma and is different from naturally occurring POAG, it is not proper to study the pathogenesis of POAG in live animals. Thus, we included the *in vitro* experimental part including immunohistochemistry and immunofluorescence experiments of POAG animals and human TM cell experiments. Therefore, we use human-derived trabecular reticulum cells and POAG animal left eye slices to validate the analysis result, which is well represented. In addition, we analyzed the cell proportions differences in POAG and healthy macaques in scRNA atlas but not validated in each histological samples. We think this phenomenon may be due to TM tissue sampling and the single-cell dissociation and filtration process. Currently, we are also actively looking for new animal models of naturally occurring POAG monkeys. In addition, we would like to verify the function of TPM1 in trabecular networks and make full use of single-cell sequencing data in the future studies.

STAR★METHODS

Detailed methods are provided in the online version of this paper and include the following:

- KEY RESOURCES TABLE
- RESOURCE AVAILABILITY
  - Lead contact
  - Materials availability
  - Data and code availability
- EXPERIMENTAL MODEL AND STUDY PARTICIPANT DETAILS
  - Ethics approval and consent to participate
  - Consent for publication
- METHOD DETAILS
  - Screening of spontaneous glaucoma in cynomolgus macaque monkeys
  - Extraction of the TM tissue
  - Single cell dissociation
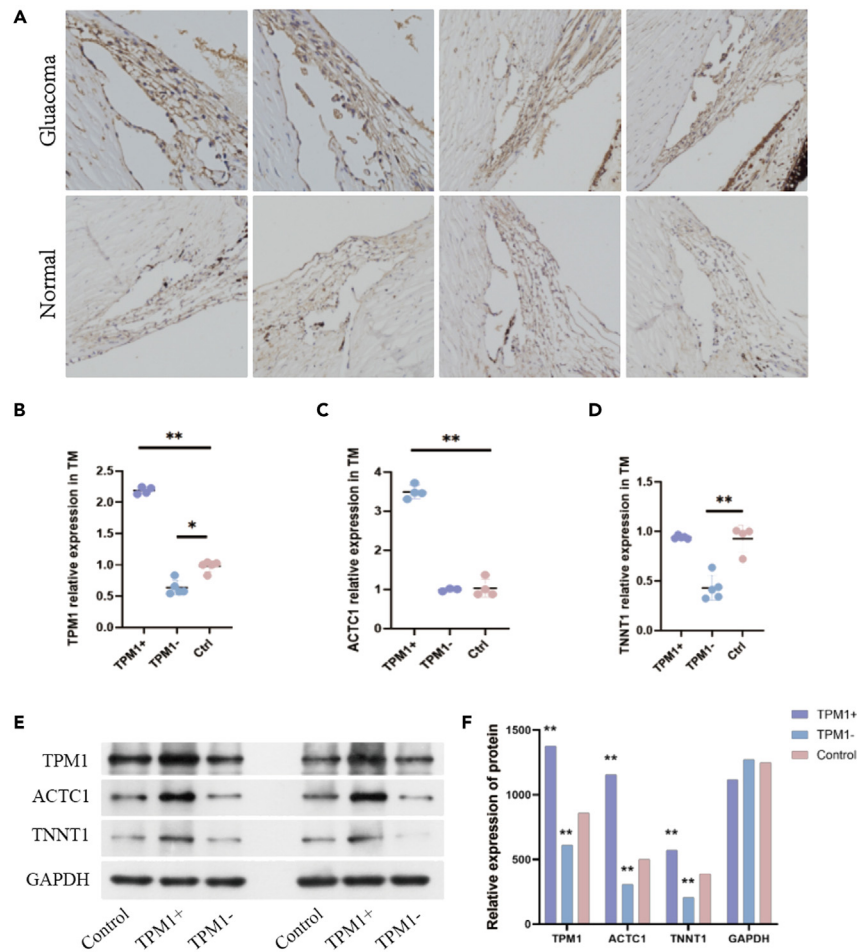
Figure 6. Exploring tissue contraction function in in macaque TM tissues and from human TM cells

(A) The TM structure of POAG and normal macaques. In the figures we can see the sieve-like regions of TM were compact and collapsed, especially in the anterior section. In the figures of normal macaques we can see the integral sieve-like structures of TM were loose and of normal thickness.

(B–D) TPM1 expression in overexpression and knockdown C:ACTC1 relative expression in TM (qPCR). TPM1 overexpression elevated ACTC1 expression (p < 0.01) D: TNNT1 relative expression in TM (qPCR). TPM1 inhibition reduced TNNT1 expression (p < 0.01).

(E and F) In the elevated TPM1 expression group, the expression level of ACTC1 protein was significantly increased, and the expression level of TNNT1 protein was also increased in a certain degree (p < 0.01). In the group with decreased TPM1 expression, the expression level of ACTC1 protein was decreased than normal group, and the expression level of TNNT1 protein was significantly decreased (p < 0.01).

- ○ Barcoding and library construction
- ○ Computational analysis
- ○ Immunohistochemistry and immunofluorescence
- ○ Human TM cell culture and TPM1 transfection
- ○ Q-PCR verification about DEGs
- ○ Western-blot experiment about DEGs
- ● QUANTIFICATION AND STATISTICAL ANALYSIS

SUPPLEMENTAL INFORMATION

Supplemental information can be found online at https://doi.org/10.1016/j.isci.2023.108024.

ACKNOWLEDGMENTS

AUTHOR CONTRIBUTIONS

Conceptualization: XJ, YHZ, WRS conceived and designed the experiments. XJ, JW, and XHC performed the experiments. All authors analyzed the data. XJ, JW, and XHC wrote the manuscript. All authors read and approved the final manuscript.

DECLARATION OF INTERESTS

The authors declare that they have no competing interests.

REFERENCES

1. Gordon, M.O., Beiser, J.A., Brandt, J.D., Heuer, D.K., Higginbotham, E.J., Johnson, C.A., Keltner, J.L., Miller, J.P., Parrish, R.K., 2nd, Wilson, M.R., and Kass, M.A. (2002). The Ocular Hypertension Treatment Study: baseline factors that predict the onset of primary open-angle glaucoma. Arch. Ophthalmol. *120*, 714–720. , discussion 829–730. https://doi.org/10.1001/archopht.120.6.714.

2. Heijl, A., Leske, M.C., Bengtsson, B., Hyman, L., Bengtsson, B., and Hussein, M.; Early Manifest Glaucoma Trial Group (2002). Reduction of intraocular pressure and glaucoma progression: results from the Early Manifest Glaucoma Trial. Arch. Ophthalmol. *120*, 1268–1279. https://doi.org/10.1001/archopht.120.10.1268.

3. The Advanced Glaucoma Intervention Study (AGIS): 7 (2000). The relationship between control of intraocular pressure and visual field deterioration. AGIS Invest. *130*, 429–440. https://doi.org/10.1016/s0002-9394(00)00538-9.

4. Stamer, W.D., and Clark, A.F. (2017). The many faces of the trabecular meshwork cell. Exp. Eye Res. *158*, 112–123. https://doi.org/10.1016/j.exer.2016.07.009.

5. Tamm, E.R. (2009). The trabecular meshwork outflow pathways: structural and functional aspects. Exp. Eye Res. *88*, 648–655. https://doi.org/10.1016/j.exer.2009.02.007.

6. Adams, C.M., Stacy, R., Rangaswamy, N., Bigelow, C., Grosskreutz, C.L., and Prasanna, G. (2018). Glaucoma - Next Generation Therapeutics: Impossible to Possible. Pharm. Res. (N. Y.) *36*, 25. https://doi.org/10.1007/s11095-018-2557-4.

7. Stamer, W.D., and Acott, T.S. (2012). Current understanding of conventional outflow dysfunction in glaucoma. Curr. Opin. Ophthalmol. *23*, 135–143. https://doi.org/10.1097/ICU.0b013e32834ff23e.

8. McDougal, D.H., and Gamlin, P.D. (2015). Autonomic control of the eye. Compr. Physiol. *5*, 439–473. https://doi.org/10.1002/cphy.c140014.

9. Buffault, J., Labbé, A., Hamard, P., Brignole-Baudouin, F., and Baudouin, C. (2020). The trabecular meshwork: Structure, function and clinical implications. A review of the literature. J. Fr. Ophtalmol. *43*, e217–e230. https://doi.org/10.1016/j.jfo.2020.05.002.

10. Klein, A.M., Mazutis, L., Akartuna, I., Tallapragada, N., Veres, A., Li, V., Peshkin, L., Weitz, D.A., and Kirschner, M.W. (2015). Droplet barcoding for single-cell transcriptomics applied to embryonic stem cells. Cell *161*, 1187–1201. https://doi.org/10.1016/j.cell.2015.04.044.

11. Jaitin, D.A., Kenigsberg, E., Keren-Shaul, H., Elefant, N., Paul, F., Zaretsky, I., Mildner, A., Cohen, N., Jung, S., Tanay, A., and Amit, I. (2014). Massively parallel single-cell RNA-seq for marker-free decomposition of tissues into cell types. Science *343*, 776–779. https://doi.org/10.1126/science.1247651.

12. Chen, M., Yu, X., Xu, J., Ma, J., Chen, X., Chen, B., Gu, Y., and Wang, K. (2019). Association of Gene Polymorphisms With Primary Open Angle Glaucoma: A Systematic Review and Meta-Analysis. Invest. Ophthalmol. Vis. Sci. *60*, 1105–1121. https://doi.org/10.1167/iovs.18-25922.

13. Aung, T., and Khor, C.C. (2016). Glaucoma Genetics: Recent Advances and Future Directions. Asia. Pac. J. Ophthalmol. *5*, 256–259. https://doi.org/10.1097/apo.0000000000000229.

14. Weinreb, R.N., and Khaw, P.T. (2004). Primary open-angle glaucoma. Lancet *363*, 1711–1720. https://doi.org/10.1016/s0140-6736(04)16257-0.

15. Geeves, M.A., Hitchcock-DeGregori, S.E., and Gunning, P.W. (2015). A systematic nomenclature for mammalian tropomyosin isoforms. J. Muscle Res. Cell Motil. *36*, 147–153. https://doi.org/10.1007/s10974-014-9389-6.

16. Wang, H.W., Liu, J., Zhao, J., Lin, L., Zhao, W.P., Tan, P.P., Tian, W.S., and Zhou, B.H. (2018). Ca(2+) metabolic disorder and abnormal expression of cardiac troponin involved in fluoride-induced cardiomyocyte damage. Chemosphere *201*, 564–570. https://doi.org/10.1016/j.chemosphere.2018.03.053.

17. Meng, L.B., Shan, M.J., Qiu, Y., Qi, R., Yu, Z.M., Guo, P., Di, C.Y., and Gong, T. (2019). TPM2 as a potential predictive biomarker for atherosclerosis. Aging (Albany NY) *11*, 6960–6982. https://doi.org/10.18632/aging.102231.

18. Deng, S., Wang, M., Yan, Z., Tian, Z., Chen, H., Yang, X., and Zhuo, Y. (2013). Autophagy in retinal ganglion cells in a rhesus monkey chronic hypertensive glaucoma model. PLoS One *8*, e77100. https://doi.org/10.1371/journal.pone.0077100.

19. McGrady, N.R., Minton, A.Z., Stankowska, D.L., He, S., Jefferies, H.B., and Krishnamoorthy, R.R. (2017). Upregulation of the endothelin A (ETA) receptor and its association with neurodegeneration in a rodent model of glaucoma. BMC Neurosci. *18*, 27. https://doi.org/10.1186/s12868-017-0346-3.

20. Patel, G., Fury, W., Yang, H., Gomez-Caraballo, M., Bai, Y., Yang, T., Adler, C., Wei, Y., Ni, M., Schmitt, H., et al. (2020). Molecular taxonomy of human ocular outflow tissues defined by single-cell transcriptomics. Proc. Natl. Acad. Sci. USA *117*, 12856–12867. https://doi.org/10.1073/pnas.2001896117.

21. van Zyl, T., Yan, W., McAdams, A., Peng, Y.R., Shekhar, K., Regev, A., Juric, D., and Sanes, J.R. (2020). Cell atlas of aqueous humor outflow pathways in eyes of humans and four model species provides insight into glaucoma pathogenesis. Proc. Natl. Acad. Sci. USA *117*, 10339–10349. https://doi.org/10.1073/pnas.2001250117.

22. Tellios, N., Belrose, J.C., Tokarewicz, A.C., Hutnik, C., Liu, H., Leask, A., Motolko, M., Iijima, M., and Parapuram, S.K. (2017). TGF-beta induces phosphorylation of phosphatase and tensin homolog: implications for fibrosis of the trabecular meshwork tissue in glaucoma. Sci. Rep. *7*, 812. https://doi.org/10.1038/s41598-017-00845-x.

23. Nakamura, N., Honjo, M., Yamagishi, R., Igarashi, N., Sakata, R., and Aihara, M. (2021). Effects of selective EP2 receptor agonist, omidenepag, on trabecular meshwork cells, Schlemm's canal endothelial cells and ciliary muscle contraction. Sci. Rep. *11*, 16257. https://doi.org/10.1038/s41598-021-95768-z.

24. Goel, M., Sienkiewicz, A.E., Picciani, R., Lee, R.K., and Bhattacharya, S.K. (2011). Cochlin induced TREK-1 co-expression and annexin A2 secretion: role in trabecular meshwork cell elongation and motility. PLoS One *6*, e23070. https://doi.org/10.1371/journal.pone.0023070.

25. Croft, M.A., Lütjen-Drecoll, E., and Kaufman, P.L. (2017). Age-related posterior ciliary muscle restriction - A link between trabecular meshwork and optic nerve head

pathophysiology. Exp. Eye Res. *158*, 187–189. https://doi.org/10.1016/j.exer.2016.07.007.

26. Wilson, S.E. (2020). Corneal myofibroblasts and fibrosis. Exp. Eye Res. *201*, 108272. https://doi.org/10.1016/j.exer.2020.108272.

27. Shinde, A.V., Humeres, C., and Frangogiannis, N.G. (2017). The role of alpha-smooth muscle actin in fibroblast-mediated matrix contraction and remodeling. Biochim. Biophys. Acta, Mol. Basis Dis. *1863*, 298–309. https://doi.org/10.1016/j.bbadis.2016.11.006.

28. Man, Y., Yi, C., Fan, M., Yang, T., Liu, P., Liu, S., and Wang, G. (2022). Identification of a novel missense mutation in the TPM1 gene via exome sequencing in a Chinese family with dilated cardiomyopathy: A case report and literature review. Medicine (Baltim.) *101*, e28551. https://doi.org/10.1097/MD.0000000000028551.

29. Bareja, I., Wioland, H., Janco, M., Nicovich, P.R., Jégou, A., Romet-Lemonne, G., Walsh, J., and Böcking, T. (2020). Dynamics of Tpm1.8 domains on actin filaments with single-molecule resolution. Mol. Biol. Cell *31*, 2452–2462. https://doi.org/10.1091/mbc.E19-10-0586.

30. Khodyuchenko, T., Zlotina, A., Pervunina, T., Zverev, D., Malashicheva, A., and Kostareva, A. (2015). Congenital heart defects are rarely caused by mutations in cardiac and smooth muscle actin genes. BioMed Res. Int. *2015*, 127807. https://doi.org/10.1155/2015/127807.

31. Song, Y., Zhao, M., Xie, Y., Zhu, T., Liang, W., Sun, B., Liu, W., Wu, L., Lu, G., Li, T.S., et al. (2019). Bmi-1 high-expressing cells enrich cardiac stem/progenitor cells and respond to heart injury. J. Cell Mol. Med. *23*, 104–111. https://doi.org/10.1111/jcmm.13889.

32. Moran, C.M., Garriock, R.J., Miller, M.K., Heimark, R.L., Gregorio, C.C., and Krieg, P.A. (2008). Expression of the fast twitch troponin complex, fTnT, fTnI and fTnC, in vascular smooth muscle. Cell Motil Cytoskeleton *65*, 652–661. https://doi.org/10.1002/cm.20291.

33. Dube, D.K., McLean, M.D., Dube, S., and Poiesz, B.J. (2014). Translational control of tropomyosin expression in vertebrate hearts. Anat. Rec. *297*, 1585–1595. https://doi.org/10.1002/ar.22978.

34. Toyota, N., Fujitsuka, C., Ishibashi, G., S Yoshida, L., Takano-Ohmuro, H., and Takano-Ohmuro, H. (2016). Morphological Modifications in Myofibrils by Suppressing Tropomyosin 4alpha in Chicken Cardiac Myocytes. Cell Struct. Funct. *41*, 45–54. https://doi.org/10.1247/csf.15007.

35. Shibata, S., Shibata, N., Ohtsuka, S., Yoshitomi, Y., Kiyokawa, E., Yonekura, H., Singh, D.P., Sasaki, H., and Kubo, E. (2021). Role of Decorin in Posterior Capsule Opacification and Eye Lens Development. Cells *10*, 863. https://doi.org/10.3390/cells10040863.

36. Raghunathan, V., Eaton, J.S., Christian, B.J., Morgan, J.T., Ver Hoeve, J.N., Yang, C.Y.C., Gong, H., Rasmussen, C.A., Miller, P.E., Russell, P., et al. (2017). Biomechanical, ultrastructural, and electrophysiological characterization of the non-human primate experimental glaucoma model. Sci. Rep. *7*, 14329. https://doi.org/10.1038/s41598-017-14720-2.

37. Lütjen-Drecoll, E., Wiendl, H., and Kaufman, P.L. (1998). Acute and chronic structural effects of pilocarpine on monkey outflow tissues. Trans. Am. Ophthalmol. Soc. *96*, 171–191. discussion 192-175.

38. Kasetti, R.B., Patel, P.D., Maddineni, P., and Zode, G.S. (2020). Ex-vivo cultured human corneoscleral segment model to study the effects of glaucoma factors on trabecular meshwork. PLoS One *15*, e0232111. https://doi.org/10.1371/journal.pone.0232111.

39. Keller, K.E., Bhattacharya, S.K., Borrás, T., Brunner, T.M., Chansangpetch, S., Clark, A.F., Dismuke, W.M., Du, Y., Elliott, M.H., Ethier, C.R., et al. (2018). Consensus recommendations for trabecular meshwork cell isolation, characterization and culture. Exp. Eye Res. *171*, 164–173. https://doi.org/10.1016/j.exer.2018.03.001.

STAR★METHODS

KEY RESOURCES TABLE

REAGENT or RESOURCE	SOURCE	IDENTIFIER
Antibodies		
HRP-conjugated Monoclonal Mouse Anti-glyceraldehyde-3-phosphate Dehydrogease (GAPDH)	Aksomics	RRID: AB_2631280
HRP-conjugated Monoclonal Mouse Anti-beta Actin	Aksomics	RRID: AB_2847811
FITC Goat Anti-Rabbit	Servicebio	RRID: AB_2904189
HRP Goat Anti-Rabbit	Servicebio	RRID: AB_2811189
Goat Anti-Rabbit IgG(H + L), Mouse/Human ads-HRP	southern biotech	RRID: AB_2795955
Rabbit Anti-Goat IgG(H + L)-HRP	southern biotech	RRID: AB_2796231
Rabbit Anti-Mouse IgG(H + L)-HRP	southern biotech	RRID: AB_2796243
Pan-Tropomyosin Polyclonal Antibody (TPM1)	Bioss	RRID: AB_3065268
Actin alpha cardiac muscle 1 Antibody (ACTC1)	Bioss	RRID: AB_3065269
Troponin T1, Slow Skeletal Muscle Antibody (TNNT1)	Bioss	RRID:AB_3065266
Deposited data		
Raw scRNA-seq data	This paper	GSE231749
Software and algorithms		
cellranger	10x Genomic	https://support.10xgenomics.com/single-cell-gene-expression/software/pipelines/latest/installation
R Programming Language	The R Foundation	r-project.org
Seurat	The R package	https://satijalab.org/seurat
functional enrichment analysis	David's website	https://david.ncifcrf.gov/home.jsp

RESOURCE AVAILABILITY

Lead contact

Further information and requests for resources and reagents should be directed to and will be fulfilled by the Lead Contact, YHZ (zhuoyh@mail.sysu.edu.cn).

Materials availability

This study did not produce any new unique reagents or mouse strains. All materials used are available through the information in the key resources table. Please contact the primary contact for more information or to request resources and reagents.

Data and code availability

- Data: All data generated or analyzed during this study are included in this published article. All single cell data were uploaded to the GEO (GSE231749).
- Code: All code is written in R. The R packages used are shown in the key resources table.
- Any additional information about the data in this article can be obtained from the lead contact.

EXPERIMENTAL MODEL AND STUDY PARTICIPANT DETAILS

All the animals were purchased from Huazhen Animal Feeding Center (Guangdong, China) following the Declaration of Helsinki (ARVO). This study was approved by the Animal Care and Treatment Committee of Zhongshan Ophthalmic Center of Sun Yat-sen University (No.2020-168). All experiments were performed under laboratory animal care guidelines to minimize animal stress and distress.

Ethics approval and consent to participate

All the animals were purchased from Huazhen Animal Feeding Center (Guangdong, China) in accordance with the Declaration of Helsinki (ARVO). This study was approved by Animal Care and Treatment Committee of Zhongshan Ophthalmic Center (ZOC) of Sun Yat-sen

University (No.2020-168). All experiments were performed in accordance with laboratory animal care guidelines to minimize animal stress and distress.

Consent for publication

Not applicable.

METHOD DETAILS

Screening of spontaneous glaucoma in cynomolgus macaque monkeys

More than 600 macaque monkeys were examined for IOP (Tono-Vet) in both eyes to screen for spontaneous glaucoma models. Those with an IOP higher than 25 mmHg have further undergone slit-lamp exams, gonioscope exams, fundus imaging as well as OCT (Figure 1, Step 1). Besides, those with other ocular diseases or systemic diseases were ruled out. Moreover, the monkeys were re-examined after 2 weeks and 1 month of the initial tests to validate the glaucoma diagnosis further. Finally, we identified 3 monkeys as spontaneous POAG models (Table 1). Another 3 healthy monkeys were selected as the control group.

Extraction of the TM tissue

The right eyes of POAG monkeys and healthy controls were used for scRNAseq analysis, while all the fellow eyes were used for subsequent experiments. The animals were euthanized by an intravenous overdose of pentobarbital sodium (50 mg/kg, Yaxin Pharmaceutical Co. Ltd, China) injection. Both eyes of each animal were enucleated, transported to the laboratory on ice within 4 h of death, and processed immediately. According to the guidance of "Consensus recommendations for trabecular meshwork cell isolation, characterization and culture",[39] a cut around the pars plana was first performed to remove the posterior segment. Next, the cornea, lens, iris, and ciliary body were removed. Vertical cuts were performed with a scalpel down from the anterior chamber/TM side toward the sclera – along the anterior and posterior margins of the TM, trying to clip the two edges of SC. Using fine-tipped forceps, the TM was lifted out and isolated (Figure 1, Step 3).

Single cell dissociation

Three POAG monkey's TM tissues were pooled together as the POAG group and three healthy monkey's TM tissues were pooled together as the control group. The TM tissues were placed in tissue preservation solution and transported to the laboratory at 4°C. The sample was removed from the tissue preservation solution and transferred to a pre-cooled 5 mL centrifuge tube. Then, the tissues were digested and incubated in 5 mg collagenase. A dissolved in human albumin at 37°C on a shaker and gently mechanically dissociated with a pipette for 20 min. Subsequently, dissociated cells were resuspended in 0.04% nonacetylated BSA and filtered through a 70 μm filter to achieve the maximum number of cells. Viability and cell number were assessed via Trypan Blue (ThermoFisher, USA) and an automatic cell counter Countstar, China). They added PBS (with 0.4% BSA) to adjust the cell concentration to barcoding requirements and library construction (around 1.0×10^{6} cells/mL).

Barcoding and library construction

Following counting, the appropriate volume for each sample was calculated for a target capture of 10000 cells and was loaded onto the 10x Genomics single-cell-A chip. After droplet generation, samples were transferred onto a pre-chilled 8-well tube (Eppendorf, USA), heat-sealed, and reverse transcription was performed using a Veriti 96-well thermal cycler (Thermo Fisher, USA). After the reverse transcription, cDNA was recovered using the Recovery Agent provided by 10x followed by a Silane DynaBead clean-up (Thermo Fisher, USA) as outlined in the user guide. Purified cDNA was amplified for 12 cycles before being cleaned using SPRIselect beads (Beckman, USA). Samples were diluted 4:1 and run on a Bioanalyzer (Agilent Technologies, USA) to determine cDNA concentration. cDNA libraries were prepared as outlined by the Single Cell 3′ Reagent Kits v3 user guide with appropriate modifications to the PCR cycles based on the calculated cDNA concentration (as recommended by 10X Genomics).

Computational analysis

We perform demultiplex and alignment for the sequencing data with the CellRanger software (10X Genomics) and monkey reference genome (Macaca Mulatta-Mmul8, Macaca Fascicularis-MacFas5). Sequenced data was processed using CellRanger software (version 4.0; 10X Genomics). The count pipeline in the CellRanger Software Suite was applied to demultiplex and barcode the sequences. The sequencer we used is Illumina NovaSeq 6000. The average sequencing coverage of sequencing was 21.86%. Q30 Bases in barcodes, RNA reads and UMI are above 90%. Based on the calculation of the single-cell expression matrix by CellRanger, filtration, normalization, dimensionality reduction, clustering, and differential gene expression analysis were conducted using the Seurat package (version 3.0). The "NormalizeData" function was used to log-normalize the counts of each cell. Dimensionality was achieved by PCA. The "FindNeighbors" and "FindClusters" functions were used to identify significant clusters at an appropriate resolution. Cells were visualized using a 2-dimensional t-SNE algorithm based on the "RunTSNE" function. The function "FindAllMarkers" was used to determine marker genes of each significant cluster. The names of each cell cluster were annotated using pieces of literature,[20,21] GeneCards, and PanglaoDB websites. For each cell type between the two groups, differential expression analysis was performed using the Wilcoxon rank-sum test as implemented in the "FindMarkers" function of the Seurat package (version 3.0). A glaucoma-related DEG dataset was established (adj P-value <0.05, Log2FC > 0.25) after identification of DEGs

between groups. The DEGs of each cell cluster were analyzed by functional enrichment analysis on Metascape and David's website (https://david.ncifcrf.gov/home.jsp) to find the pathways and genes related to the functions of TM (Figure 4, Step 4).

Immunohistochemistry and immunofluorescence

Each eye of the monkeys was paraffin-embedded, sagittally sectioned, deparaffinized following xylene and 100% ethanol incubations, and antigen-retrieved in boiling citric acid buffer for 15 min. Blocking buffer was prepared with 5% normal serum, 1% bovine serum albumin, and 0.025% Triton X- in tris-buffered saline. Sections were incubated in a blocking buffer at room temperature (RT) for 1 h. Immunohistochemistry experiments were performed in the fellow eyes of all the monkeys. Sections were incubated with the anti-TPM1 antibody (Bioss, Bs-9622R, 1:100)for 1 h. Negative controls were additionally obtained by omitting each primary antibody. After washing, secondary antibodies were incubated with 100 g/mL diamidino-phenyl-indole (DAPI, Sigma) added to each section for 30 min. Sections were washed and coverslipped, while photographs were acquired with a confocal microscope (Leica DM 2500 SPE). Sections were fixed in 4% PFA, blocked with 0.5% BSA with 0.3% Triton X-100 in PBS, and then incubated overnight at 4°C with anti-ACTC1 antibody (Bioss, Bs-17012R, 1:100) or anti-TNNT1 antibody(Bioss, Bs-10616R, 1:100). The secondary antibodies in this study were Alexa Fluor 647 goat anti-human antibody and Alexa Fluor 488 goat anti-human antibody. Negative controls were additionally obtained by omitting each primary antibody. Finally, the sections were counterstained with DAPI (AnaSpec/Eurogentec Group) and mounted with Fluoromount-G (SouthernBiotech, Birmingham, AL, USA). Photographs were acquired with a confocal microscope (Leica DM 2500 SPE).

Human TM cell culture and TPM1 transfection

We used human TM primary cells to explore the effect of altered TPM1 levels on ACTC1 and TNNT1 levels. Then, a plasmid containing the TPM1 overexpression construct or the gene knockdown construct were transfected into cells using Lipo3000 transfection reagent. Twenty-four hours after transfection, successful gene transfection was judged by identification of transfection efficiency using an inverted fluorescence microscope.

Q-PCR verification about DEGs

RNA was extracted from TPM1 overexpression TM cells, TPM1 repressed expression of TM cells, normal TM cells and trabecular meshwork cells. The expression of TPM, ACTC1, and TNNT1 markers was evaluated by the Quanti Nova SYBR Green PCR Kit with specific primers on a LightCycler480 (Roche). A housekeeping gene (ACTB) was used for normalization.

Western-blot experiment about DEGs

100 μL of lysis solution (containing PMSF and Cocktail) was added to each tube of cells and lysed on ice for 30 min. Centrifuged at 14,000 rpm for 5 min at 4°C after lysis, the centrifuged supernatant was transferred to a centrifuge tube and stored at −80°C. The protein solution of the samples and 5 × loading buffer were mixed at 4:1, boiled for 10 min, slowly returned to room temperature, and stored at −20°C after slightly centrifuged. 2 μL of each sample was diluted 20-fold with 38 μL H2O. 20 μL of diluted standard samples and experimental samples were taken to a 96-well plate, and a 200 μL working solution was added to each well. The absorbance value was read in a microplate at a wavelength of 560 nm. 1 × electrophoresis buffer was added into the upper and lower electrophoresis tanks, and the liquid level of buffer in the upper tank shall exceed the top of the loading well. 80V constant voltage electrophoresis until bromophenol blue reached the separation, 100 V constant voltage electrophoresis until bromophenol blue just came out of the bottom of the gel. The gel was removed and placed on filter paper to form the structure as a gel transfer stack, filter paper, gel, PVDF membrane, filter paper, and gel transfer stack.100V constant pressure was transferred at a low temperature according to the molecular protein weight per kDa for 1 min. The hybridization membrane was removed and rinsed in TBST for 5 min once. The 5% nonfat dry milk solution was blocked for 2 h at room temperature. Membranes were washed with TBST for 8 min once. Appropriate primary antibody dilution concentration overnight at 4°C. Membranes with TBST were washed for 8 min 3 times. The corresponding secondary antibody diluent was incubated at 37°C for 50 min–3 h, washed membranes with TBST for 8 min, 3 times. The hybridization membrane was placed on a transparent plastic plate, not allowing the membrane to dry. The chemoluminescence substrate was applied evenly to the surface of the membrane with a clean pipette and allowed the reaction to continue for 1 to 5 min. The filter paper provided by the kit was used to suck off the excess substrate solution on the membrane surface and place it in the cassette.

QUANTIFICATION AND STATISTICAL ANALYSIS

The PCR analysis (Figures 6B–6D) compared the gene expression levels that were assessed in transfecting normal human TM cells with TPM1 from 3 experimental groups: a control group (n = 3), the TPM1 overexpression group (n = 3)and the TPM1 suppressor expression group (n = 3). The gene expression data was processed using the ΔΔCt method. Statistical significance was determined using a two-tailed unpaired Student's t-test, and the p value threshold for significance was set at $p < 0.05$. The mean ΔCt values and standard errors of the mean (SEM) were calculated for each group. All statistical analyses were performed using spss 29.0.

In Western blot analysis (Figures 6E and 6F), band intensities were quantified using ImageJ software. Significance was determined at a p value <0.05. The results are presented as mean values with 95% confidence intervals.